

## A Comparison of the Atmospheric Circulations Simulated by the CCM3 and CSM1\*

BYRON A. BOVILLE AND JAMES W. HURRELL

*National Center for Atmospheric Research,<sup>+</sup> Boulder, Colorado*

(Manuscript received 7 May 1997, in final form 24 September 1997)

### ABSTRACT

The atmospheric state simulated by the National Center for Atmospheric Research (NCAR) Community Climate Model, version 3 (CCM3), is compared to that simulated by the NCAR Climate System Model, version 1 (CSM1). CCM3 is an atmospheric general circulation model that uses specified sea surface temperatures (SSTs) for a lower boundary condition. Observed monthly mean SSTs for 1979–93 were used in the present study. CSM1 is a coupled general circulation model in which the SSTs are determined as part of the simulation and CCM3 serves as the atmospheric component. It is found that the differences between CCM3 and CSM1 are quite small in most measures of the atmospheric circulation, consistent with the accurate and drift-free simulation of the SSTs in the coupled model. There are substantial temperature differences near the surface in the Arctic and over the ocean around Antarctica, resulting from different sea-ice distributions. The tropical precipitation also has significant differences, although neither simulation is clearly better and the errors in the two simulations tend to have opposite signs with respect to observations. In response to the change in latent heat release the tropical divergent circulation changes significantly. Middle- and high-latitude circulation changes are modest, occurring mostly in winter in association with the sea-ice changes.

### 1. Introduction

The National Center for Atmospheric Research (NCAR) Climate System Model, version 1 (CSM1), is a new physical climate model containing coupled atmospheric and oceanic general circulation models (GCMs), a land surface biophysics model, and a sea-ice model. The atmospheric GCM is the NCAR Community Climate Model, version 3 (CCM3) (Kiehl et al. 1998a), the latest version of the NCAR Community Climate Model, which has a long history of use in atmospheric circulation studies. CCM3 can be run coupled within CSM1, with sea surface temperatures (SSTs) and ice properties determined as part of the solution, or it can be run with those properties specified from observations.

A 300-yr control simulation of CSM1 has been performed for current climate forcing conditions (Boville and Gent 1998). There is a brief (~10 yr) adjustment period in which the land surface comes to equilibrium with the ocean and atmosphere, after which the simu-

lation is remarkably free of drifts in surface temperatures (Boville and Gent 1998). The simulated SSTs are in excellent agreement with observations (see Fig. 1 over oceans). Ocean salinity and deeper ocean temperatures do show significant drifts over the course of the simulation (Bryan 1998), but do not affect the results shown here. The sea-ice distribution in the Southern Hemisphere (SH) also agrees well with observations, although the Northern Hemisphere (NH) ice is about 15% too extensive in winter and is also somewhat thicker than observed (see Fig. 2).

This study compares the atmospheric circulation in the coupled solution to that obtained in CCM3 forced with observed monthly mean SSTs for the period 1979–93. CSM1 produces a fairly accurate simulation of the SST and ice distributions, so the differences between coupled and uncoupled simulations will be shown to be modest. However, significant differences are found in the tropical precipitation and winds. Smaller changes are found in middle to high latitudes, occurring particularly in winter. The formulations of CCM3 and CSM1 are briefly summarized in section 2. Differences in circulation statistics are discussed in section 3 and conclusions are summarized in section 4.

### 2. Model formulation

#### a. CCM3

CCM3, described in Kiehl et al. (1998a), represents a significant improvement over previous versions of the

\* An electronic supplement to this article may be found on the CD-ROM accompanying this issue or at <http://www.ametsoc.org/AMS>.

<sup>+</sup> The National Center for Atmospheric Research is sponsored by the National Science Foundation.

Corresponding author address: Dr. Byron A. Boville, NCAR/CGD, P.O. Box 3000, Boulder, CO 80307-3000.  
E-mail: [bovill@ucar.edu](mailto:bovill@ucar.edu)

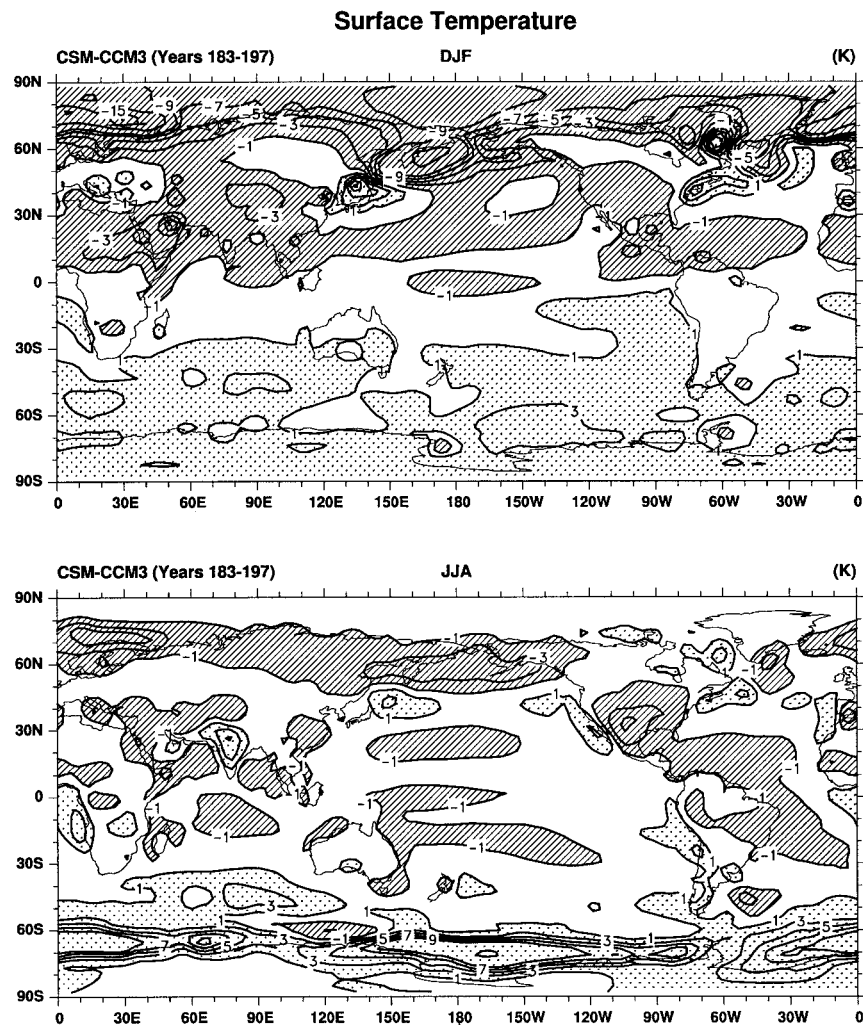


FIG. 1. Surface temperature differences (K) between CSM1 and CCM3 for DJF (top) and JJA (bottom). The contours are  $\pm 1, \pm 3, \pm 5, \dots$ ; values  $< -1$  K are hatched and values  $> +1$  K are stippled.

CCM. The ability of CCM3 to simulate the climate of the period 1979–93, when forced with the observed monthly average SSTs for that period, is discussed in Kiehl et al. (1998b), Hack et al. (1998), Hurrell et al. (1998), and Briegleb and Bromwich (1998a,b). CCM3 is a spectral model and, in the standard configuration used for the simulations discussed here, employs T42 truncation ( $\sim 2.9^\circ$ ) with 18 levels in the vertical. Deep moist convection rooted in the boundary layer is parameterized by the scheme of Zhang and McFarlane (1995), while Hack (1994) is used for shallow and non-precipitating convection. The longwave radiative effects of the principal greenhouse gases ( $\text{CO}_2$ ,  $\text{O}_3$ ,  $\text{H}_2\text{O}$ ,  $\text{CH}_4$ ,  $\text{N}_2\text{O}$ , CFC11, and CFC12) are treated using broadband approximations, and an 18-band  $\delta$ -Eddington approximation is used for solar radiation (see Kiehl et al. 1998b). The nonlocal K-profile parameterization used for boundary layer turbulent fluxes (J. J. Hack and A. A. M. Holtslag 1997, personal communication) treats

the surface layer more appropriately than the earlier scheme described by Holtslag and Boville (1993), lowering the boundary layer depths, increasing the surface humidity, and reducing the latent heat flux at the surface. The Atmospheric Model Intercomparison Project dataset (Gates 1992) is used for SSTs. In this dataset, grid boxes where a significant amount of sea ice is present are coded with a special value of SST ( $-1.8^\circ\text{C}$ ). In CCM3, such grid points are assumed to be entirely covered with 2 m of ice and 5 mm (water equivalent) of snow overlying an ocean with temperature fixed at  $-2^\circ\text{C}$ . A four-layer diffusion model is used to determine the surface temperature.

A land surface biophysics model (LSM 1.0; Bonan 1998 and references therein) is contained within CCM3 and is also invoked in CSM1. In either case, LSM runs on the same grid as CCM3 (a restriction that will be relaxed in future versions of the CSM). LSM allows differing vegetation types, bare soil, lakes, and wetlands

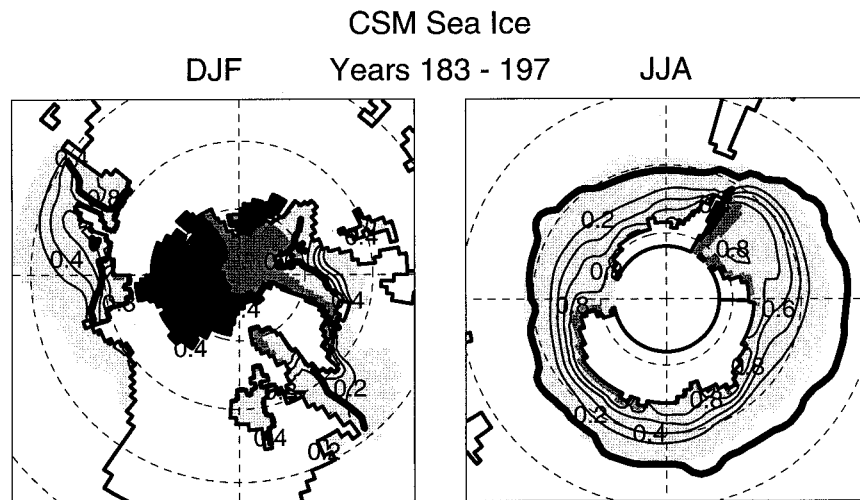


FIG. 2. Sea-ice concentration (fractional area of each grid box covered by ice) simulated by CSM1 for winter in the NH (left) and SH (right), contoured at 0.2. The three levels of shading indicate ice thickness <1, 1–3, and >3 m. The heavy solid lines show the location of the specified ice edge in CCM3 (actually the boundary of the region, which is 100% covered by ice during at least 50% of the period).

to be treated separately within each grid cell. Cell average fluxes are then determined by averaging the fluxes from each surface type according to time-independent areas for each type.

*b. CSM1*

Gent et al. (1998) describe NCAR CSM Ocean Model (NCOM), the ocean GCM used in CSM1, and Weatherly et al. (1998) describe the sea-ice model. The NCOM configuration for the present CSM1 simulation has 45 levels in the vertical (4 in the top 50 m, 25 in the top km), variable resolution in latitude (1.2° at the equator and poles, 2.3° in midlatitudes), and 2.4° resolution in longitude. The main physical parameterizations are the Gent–McWilliams eddy mixing parameterization (Gent et al. 1995) and the nonlocal K-profile boundary layer parameterization (Large et al. 1994), similar to that used in CCM3. The sea-ice model uses the same grid as NCOM. The ice dynamics employ the cavitating fluid rheology of Flato and Hibler (1992), while the ice thermodynamics are based on the three-layer model of Semtner (1976). Ice thickness and concentration are determined by the model, and snow is allowed to accumulate and melt on top of the ice.

Turbulent fluxes at the interfaces between the model components in CSM1 are computed in a separate component, the flux coupler, if they depend on the state at the interface of more than one system. In that case, state variables are interpolated to the highest resolution component model grid (the ocean grid in the present configuration) and fluxes are averaged back to the lower resolution grid.

*c. Changes to CCM3 for coupling*

CCM3 is used almost unchanged in the both the coupled and uncoupled simulations. The main difference is that the internal CCM3 subroutines to compute surface fluxes over ocean and sea ice are switched off in CSM

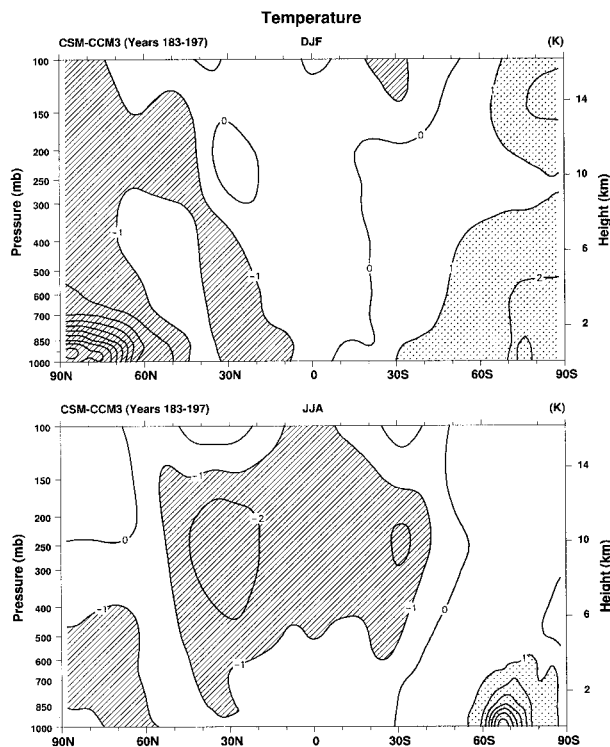


FIG. 3. Zonally averaged temperature differences between CSM1 and CCM3, for DJF (top) and JJA (bottom), contoured at 1-K intervals.

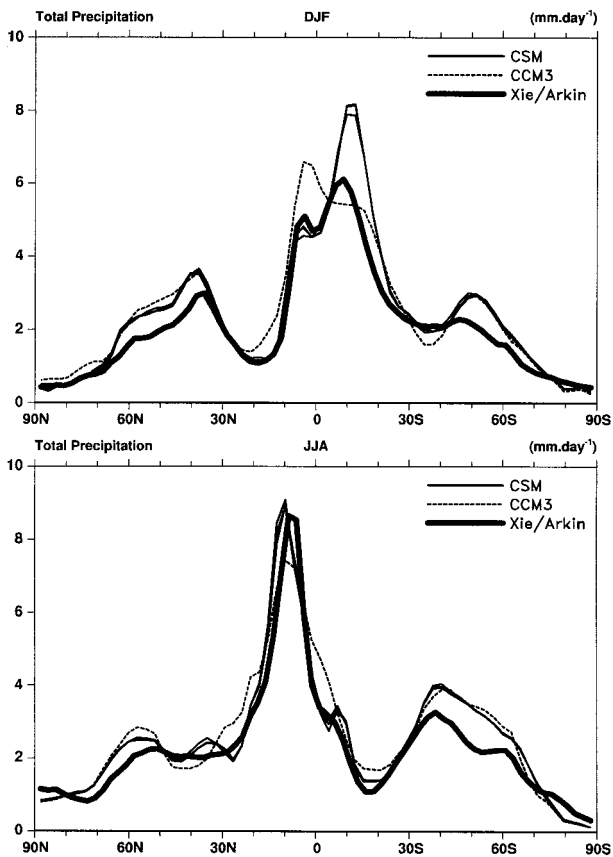


FIG. 4. Total zonally averaged precipitation rate for DJF (top) and JJA (bottom) in  $\text{mm day}^{-1}$  for CSM1, CCM3, and observations from Xie and Arkin (1996). Three CSM1 curves are shown but are almost indistinguishable (years 83–97, 183–197, and 283–297).

and the fluxes are supplied by the coupler. The same algorithms are used in both cases. A background aerosol, active in the shortwave only, is included in CCM3 with a specified, globally uniform optical depth (Kiehl et al. 1998b). The aerosol optical depth has been adjusted by experimentation to obtain a globally and annually averaged balance between incoming and outgoing radiation within less than  $1 \text{ W m}^{-2}$  in both CCM3 and CSM1. A value of 0.14 is used for the uncoupled model and 0.1 in CSM1. The differing aerosol optical depth is required primarily because the land–sea distribution is slightly different in the two model configurations, giving a different average albedo. In CSM1, the land–sea distribution is determined on the finer ocean grid and fractional land areas are allowed under atmospheric grid boxes. In CCM3, a grid box must be entirely land, ocean, or sea ice, so the resulting land–sea distribution is slightly less accurate than in CSM, although some liberties are taken with coastlines in NCOM for computational efficiency. Figure 2 shows the actual land–sea boundary used in CSM1 in middle and high latitudes.

Radiative fluxes and heating rates are determined ev-

ery hour in CCM3. Surface fluxes are also computed every hour in CSM1, on the same time step as the radiative fluxes, compared to every atmospheric time step (20 min) in CCM3. Instantaneous states and hourly averaged fluxes (e.g., downward radiative fluxes and precipitation) are passed to the coupler, where turbulent fluxes are determined and passed to the component models. Although LSM is an exception to this, in that it calculates the turbulent fluxes over land surfaces itself, the effect is the same: the atmospheric state and input fluxes are fixed over an hour; three 20-min time steps are taken; and the hourly averaged fluxes are passed to the coupler for merging with fluxes from ocean and ice surfaces. The effect of 1-h compared to 20-min flux computations is negligible in practice, as determined by 10-yr parallel simulations of the coupled system using both methods.

Apart from the fact that the SSTs in CSM are determined internally by an ocean GCM, the biggest difference between CSM and CCM3 is the use of fractional areas of different surface types in CSM. Thus, an ocean point may be partially covered by sea ice and several such points may underlie part of an atmospheric grid cell, the rest of which is land. In CCM3, a grid cell must be entirely land, ocean, or sea ice. This has a particularly large impact over the SH in winter, when extensive regions of fragmented ice occur around Antarctica, as will be seen below. The impact of fractional land–sea points is small, as determined by comparing an uncoupled CCM3 simulation using climatological SSTs with a CSM1 simulation in which climatological SSTs were specified on the NCOM grid and the sea-ice distribution was diagnosed as in CCM3. The differences were much smaller than those discussed below, and were mostly associated with the different sea-ice thermodynamic calculations.

### 3. Circulation statistics

In the following analysis, uncoupled CCM3 results are taken from the same simulation, using specified SSTs for 1979–93, as discussed in Kiehl et al. (1998a) and the other CCM3 references above. Results of several such simulations are available and the variability of the 15-yr seasonal means is small. Statistics for the 300-yr coupled simulation have been computed for three separate 15-yr periods (years 83–97, 183–197, and 293–297), although most of the results are shown below only for years 183–197. There is no significant trend in the surface temperatures in the coupled simulation and interdecadal variability is small enough (see Boville and Gent 1998) that 15-yr seasonal means are very stable, as in the uncoupled model. Season means for December–February (DJF) and June–August (JJA) are shown in all cases. For convenience, the uncoupled model will be referred to as CCM3 and the coupled model as CSM1 below.

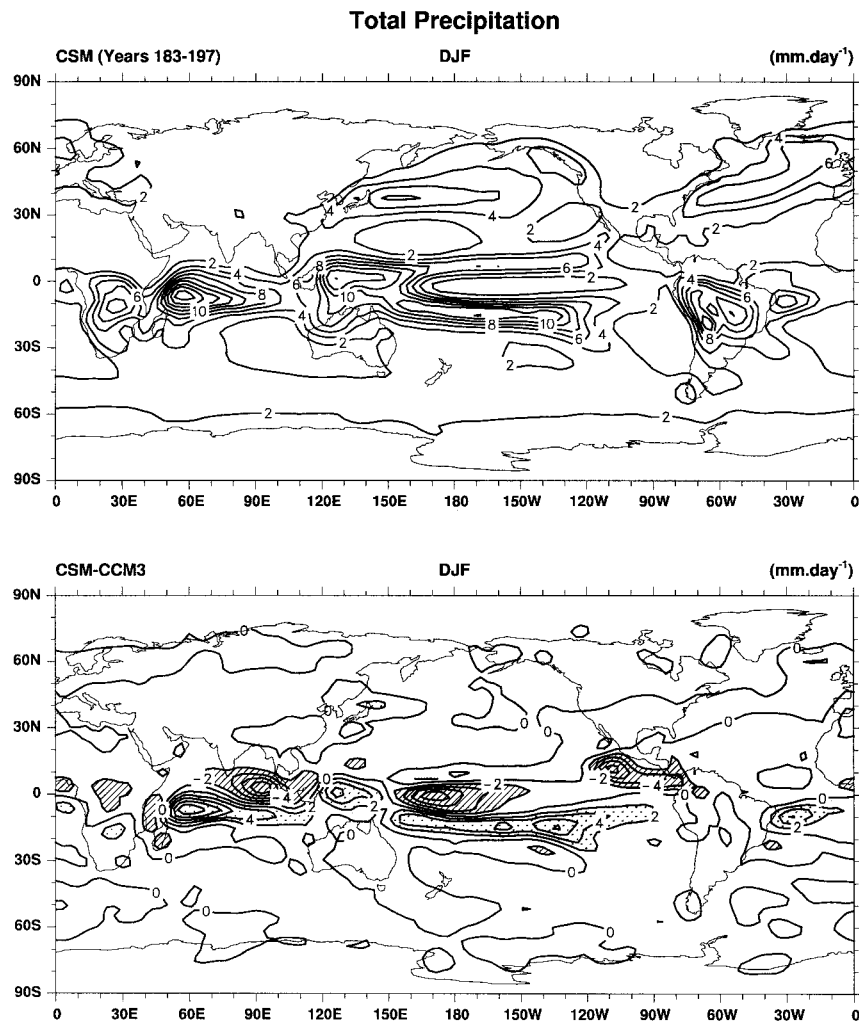


FIG. 5. Maps of the DJF total precipitation rate, contoured at 2 mm day<sup>-1</sup>, for CSM1 (top) and the difference between CSM1 and CCM3 (bottom).

*a. Temperature and sea ice*

The primary difference between CCM3 and CSM1 is that CSM predicts the SST and ice distributions instead of specifying them. Therefore, the difference in the simulated and specified surface temperatures is the quantity of fundamental importance in forcing other differences in the simulations. The global and annually averaged surface temperature in CSM1 (287.2 K) is 0.3 K colder than in CCM3 (287.5 K). Figure 1 shows the DJF and JJA surface temperature differences. The differences over low and middle latitudes are generally quite small ( $\pm 2$  K or less), although not necessarily insignificant (see below; Kiehl 1998; Meehl and Arblaster 1998). The largest differences occur in high latitudes during winter, and the sign of the differences is opposite between the two hemispheres. The high-latitude temperature differences between CSM1 and CCM3 result from differences in the ice distributions.

The winter sea-ice thickness and concentration simulated by CSM1 are shown in Fig. 2, together with the specified ice line used by CCM3. The CSM1 ice simulation is discussed extensively in Weatherly et al. (1998). The principal problems with the CSM1 ice simulation are that the ice is somewhat too thick in the Arctic Ocean (note the extensive region of thickness  $>3$  m) and extends too far into both the North Pacific and North Atlantic in DJF. The difference that can be maintained between the temperatures of the ice surface and of the seawater under the ice ( $\sim -1.8^\circ\text{C}$ ) is strongly related to the ice thickness. In addition, CSM1 allows the accumulation of snow on top of sea ice, and water equivalent values of 10 cm are typical in the Arctic compared to the 5 mm specified in CCM3. Therefore, the excessive ice thickness in the Arctic in CSM1 results in temperatures 7–10 K colder over the Arctic Ocean than in CCM3. In the North Atlantic and North Pacific,

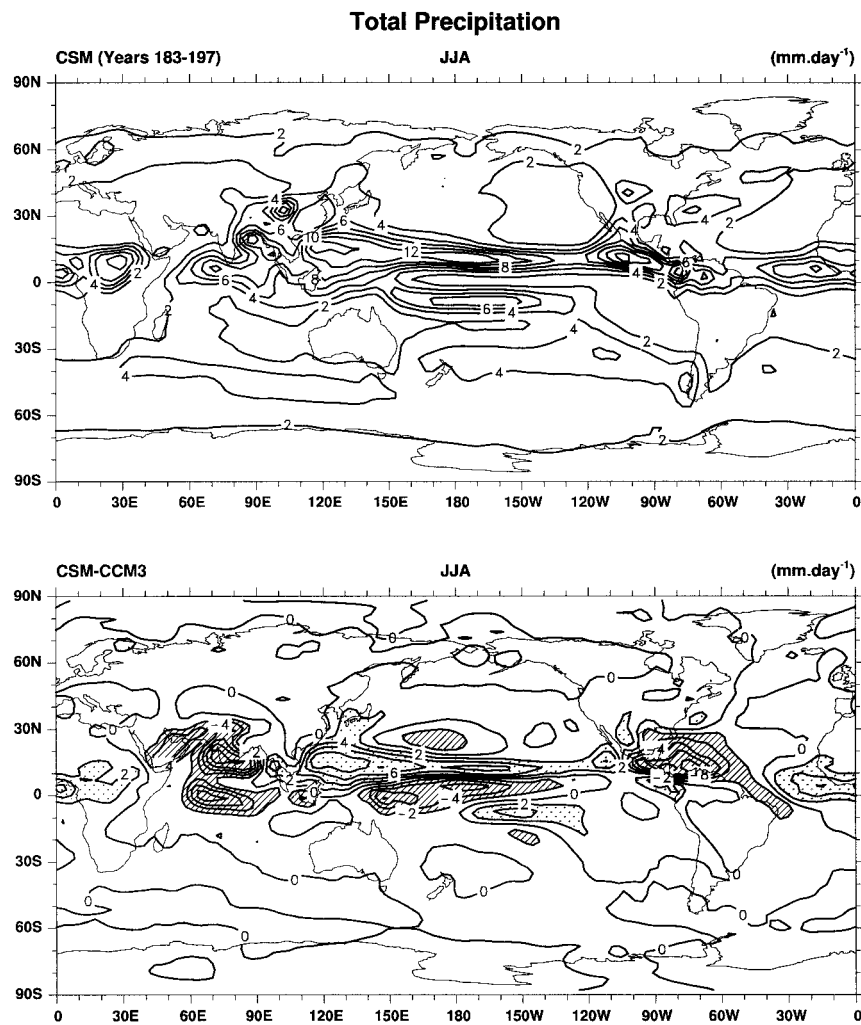


FIG. 6. As in Fig. 5 except for JJA.

the simulated ice is less than 1 m thick and much of it is not highly concentrated (generally <50%), but there is a substantial impact on the temperature. Differences reach as much as 20 K in the North Pacific and 28 K in the Barents Sea, and maximize where the ice in CSM1 is highly concentrated over regions that should be mostly ice free. The CCM3 temperatures are already colder than observed (Briegleb 1998b; Hack et al. 1998) and the bias in CSM1 is even worse.

In contrast, the SH ice simulation in CSM1 is very successful, both with regard to ice areas and thickness (see Weatherly et al. 1998). On the other hand, the sea ice diagnosed in CCM3 from the SSTs is much too extensive, since total ice coverage is assumed over large areas where loosely concentrated pack ice occurs in reality. This can be seen in Fig. 2, where the ice-covered area in CCM3 is actually larger than the extent (concentration >0) of ice in CSM1. CCM3 also uses a uniform 2-m thickness for sea ice, which is not a bad assumption in the NH, but observed ice thicknesses in the

SH pack ice are typically less than 1 m as found in CSM1. Consequently, the JJA surface temperatures around Antarctica in CSM1 are up to 15 K warmer than in CCM3 and are in better agreement with observations.

The surface temperature differences extend into the lower troposphere (Fig. 3), where CSM1 is up to 10 K colder than CCM3 near the North Pole in DJF and 7 K warmer around the coast of Antarctica in JJA. In lower latitudes and above 700 mb, the differences between CSM1 and CCM3 are small, although the NH is generally colder and the SH warmer in the coupled model. In fact, the differences in zonally averaged temperature between CSM1 and CCM3 are considerably less than the differences between CCM2 (the previous version of the CCM) and CCM3, when forced with the same SSTs. Even the high-latitude temperature differences are confined mostly within the boundary layer and do not have a major influence on the zonally averaged winds. Tropical wind differences are largely regional, rather than zonally symmetric, and will be discussed below.

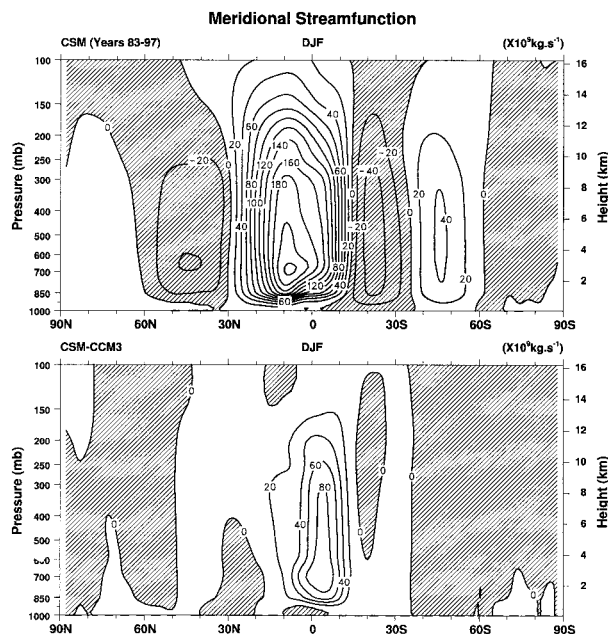


FIG. 7. DJF mean meridional streamfunction for CSM1 (top) and the difference between CSM1 and CCM3 (bottom) contoured at  $20 \times 10^9 \text{ kg s}^{-1}$ .

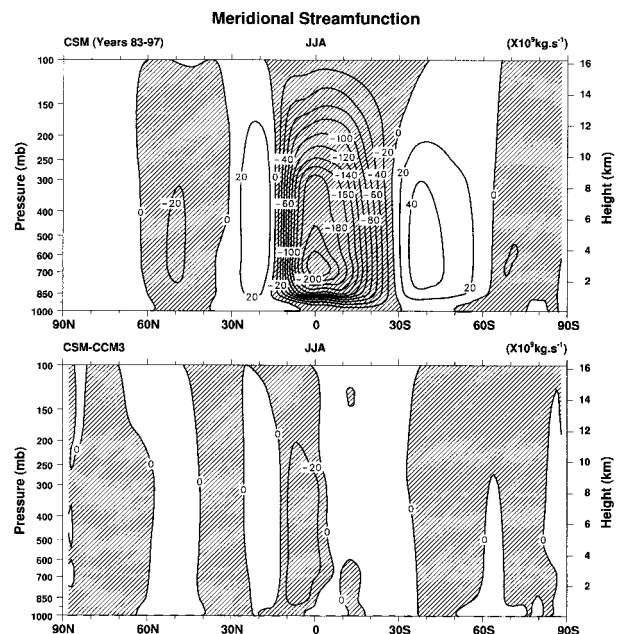


FIG. 8. As in Fig. 7 except for JJA.

*b. Precipitation*

Figure 4 shows that the zonally averaged precipitation in CSM1 is very similar to that in CCM3 outside of the Tropics. Both simulations give too much precipitation in the midlatitude storm tracks, compared to estimates from Xie and Arkin (1996). The consistency between 15-yr means is also evident in Fig. 4, where all three of the analyzed periods are shown for CSM1 and the curves lie mostly on top of each other.

Unlike midlatitudes, the tropical precipitation is significantly different between the two simulations. Although the low-latitude SST errors in CSM1 are mostly less than 1 K, relatively small errors can have significant impacts on the tropical precipitation. In DJF, both simulations show highly asymmetric intertropical convergence zones (ITCZs), while the observations show only a modest asymmetry, with maximum precipitation near 10°S. The maximum precipitation in CCM3 is too large and is north of the equator with a very broad peak extending into the SH (see Hack et al. 1998). In contrast, the precipitation rates in CSM1 have two distinct peaks separated by an equatorial minimum that closely matches the observational estimates, although the peak near 10°S is exaggerated by about 30%. In JJA, both simulations produce a single peak centered at 10°N, although the CSM1 precipitation is more latitudinally confined and the peak value is larger, in better agreement with the observations.

The maps in Figs. 5 and 6 show that the zonal-mean changes in tropical precipitation are made up of major shifts in the precipitation patterns. In DJF, CSM1 has

large precipitation maxima near 10°S in all three oceans, although the zonal mean is dominated by the Pacific basin. The southern ITCZ in the Pacific is much stronger than observational estimates of Xie and Arkin (1996) and stretches across most of the basin, while the South Pacific convergence zone (SPCZ) is notably suppressed compared to both the observations and CCM3. The precipitation is also suppressed along the equator in the western and central Pacific, where the simulated SSTs are colder than observed (Fig. 2). These are common features of coupled ocean–atmosphere GCMs, as noted by Mechoso et al. (1995). CCM3 also has a tendency to develop an excessive southern ITCZ in the Pacific, but to a lesser extent than CSM1, and does have a reasonable SPCZ. The equatorial precipitation is actually somewhat too strong in CCM3, consistent with the lack of an equatorial minimum in the zonal-mean precipitation (Fig. 4). The northern ITCZ in the Pacific is a little stronger in CSM1 than in CCM3, but is still weaker than observed across most of the basin. In the eastern Pacific, near 10°N, the magnitude of precipitation is closer to observations in CSM1, where there is a spurious maximum in CCM3. The western Pacific warm pool, analyzed in detail in Kiehl (1998), has about 50% too much precipitation in CSM1.

The DJF Indian Ocean precipitation maximum shifts to the southwest in CSM1 resulting in less precipitation north of the equator and more to the south. However, the Indian Ocean precipitation is exaggerated in both simulations compared to the observations, in which a weaker maximum extends across the whole basin. CSM1 develops a precipitation maximum in the Atlan-

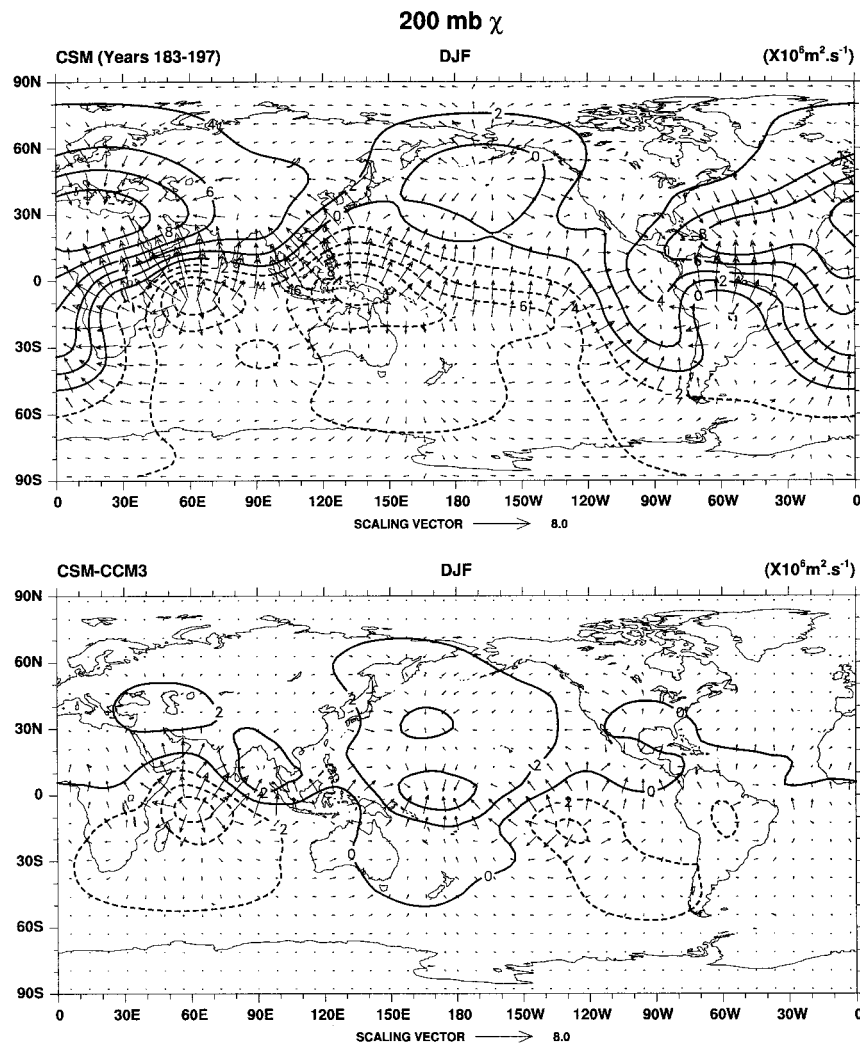


FIG. 9. Maps of the DJF velocity potential vectors at 200 mb, magnitude contoured at  $2 \times 10^6 \text{m}^2 \text{s}^{-1}$ , for CSM1 (top) and the difference between CSM1 and CCM3 (bottom).

tic, which is absent in CCM3, but the feature is located near  $10^\circ\text{S}$ , rather than along the equator as observed.

An excessive southern ITCZ persists in the Pacific even in JJA (Fig. 6), although it is much weaker than in DJF, and the SPCZ is still suppressed in the central Pacific. In the Indian and Atlantic Oceans, the JJA precipitation shifts almost entirely north of the equator. Again, the precipitation along the equator in the Pacific, where the SST is 1–2 K too cold, is suppressed in CSM1 compared to CCM3. In this season, the precipitation has mostly shifted into the vicinity of the Philippines and the northern branch of ITCZ, which extends across the entire Pacific Ocean, in better agreement with observations than in CCM3. The Atlantic ITCZ is also stronger in CSM1, with greatly reduced precipitation in the Caribbean Sea, again in better agreement with observations than CCM3. The precipitation is reduced throughout the Indian Ocean basin, representing an improvement with respect to CCM3 north of the equator,

but the equatorial precipitation is much too weak in CSM1. A spurious precipitation maximum over the southeastern Arabian Peninsula in CCM3 does not appear in CSM1.

The precipitation changes above result from tropical SST errors of only  $\sim 1$  K in CSM1 and are a mix of improvements and degradations with respect to CCM3. It is curious that the precipitation in both simulations has errors of comparable magnitude, but generally of opposite sign, with respect to the observations. One might normally expect that allowing the SSTs to respond to the atmospheric circulation would increase errors in the resulting circulation. We suspect that the tropical precipitation errors in CCM3 are sustained by erroneous surface heat fluxes, which are not compatible with realistic heat transports in the ocean. Allowing the ocean to respond causes surface temperature changes that act to suppress the erroneous fluxes. Therefore, flux errors in the uncoupled model, prob-

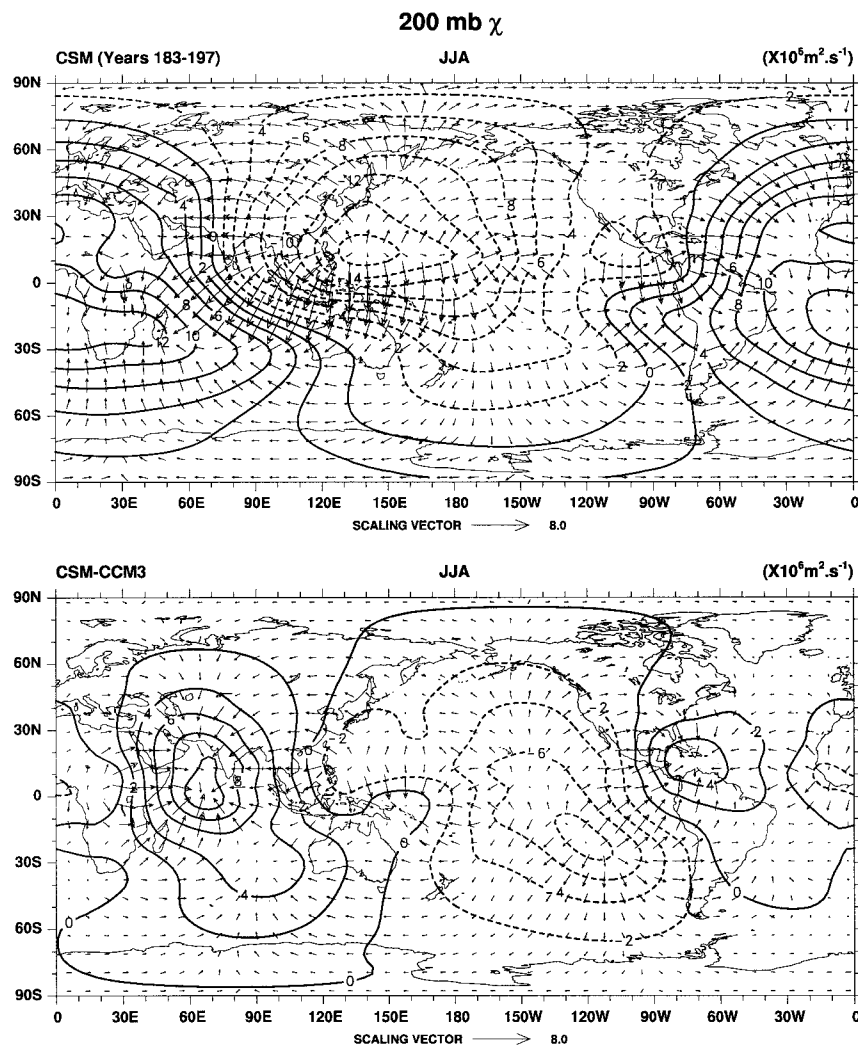


FIG. 10. As in Fig. 9 except for JJA.

ably resulting from deficiencies in the atmospheric physical parameterizations, are transformed into SST errors in the coupled model. This process is neither linear nor local (e.g., Kiehl 1998) but implies that the precipitation errors in the coupled model may actually be smaller than in the uncoupled model as long as the SST errors are not too big.

*c. Circulation*

The large-scale divergent circulation in the Tropics has significant differences between CSM1 and CCM3, associated with the changes in precipitation and latent heat release. The mean meridional circulation in the Tropics (Figs. 7 and 8) is more intense in CSM1 by about 30% in DJF and 10% in JJA, reflecting the larger changes in precipitation (Fig. 4) and increase in meridional SST gradient (cf. Fig. 1). The velocity potential at 200 mb (Figs. 9 and 10) illustrates regional changes in the large-scale divergent outflow. There is a much

larger region of upper-level divergence over the Indian Ocean during DJF in CSM1, consistent with the unrealistic shift in precipitation (Fig. 5). The other prominent features of the difference field in Fig. 9 are a strong decrease in the outflow over the equator in the western Pacific, where the convection is suppressed relative to CCM3, and an increase to the south of the equator in the eastern Pacific, where the convection is significantly increased in CSM1.

In JJA, the reduction in precipitation over the Indian Ocean and Caribbean Sea in CSM1 (Fig. 6) results in a strong reduction in the divergent outflow (Fig. 10). In the Pacific, the outflow increases somewhat near the Philippines, where the largest increase in precipitation occurs. However, the largest change is in the subtropical eastern Pacific, where there is net outflow in CSM1 and inflow in CCM3.

There is a substantial weakening of the Walker circulation in CSM1 during DJF, with a reduction in the low-level easterlies over the Pacific (Fig. 11) and a cor-

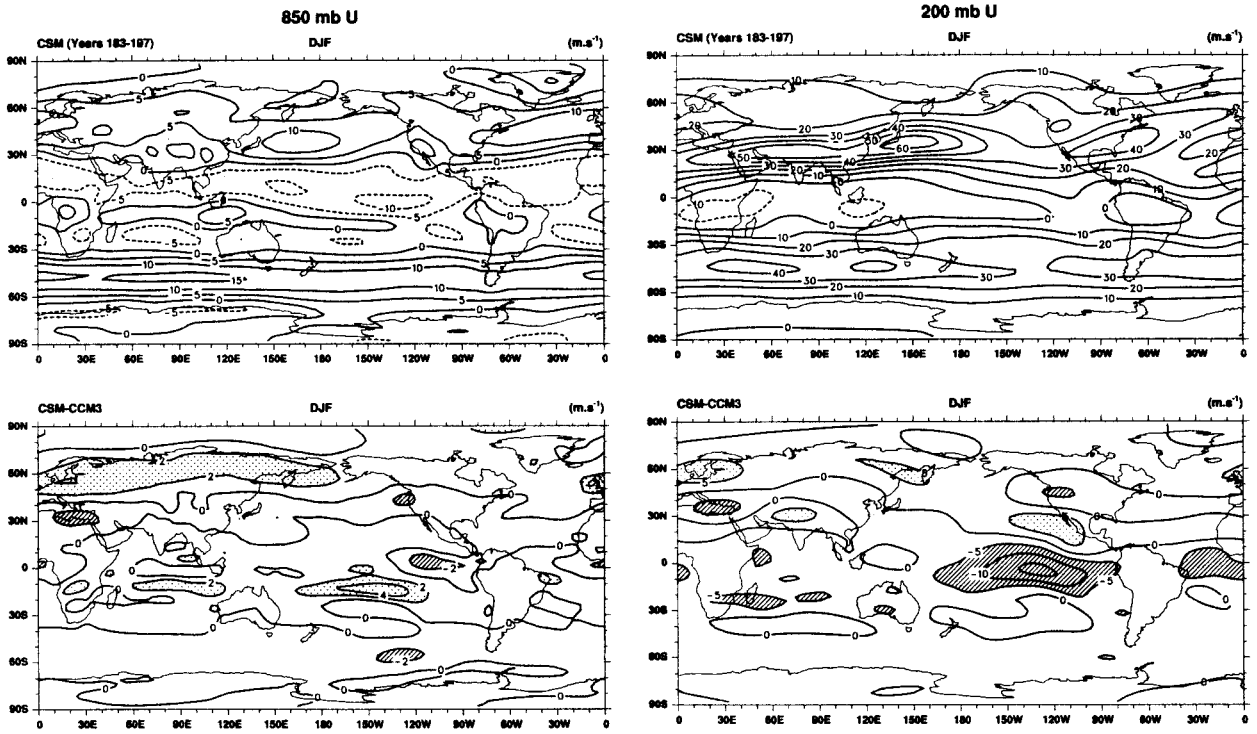


FIG. 11. Maps of DJF zonal wind in  $m s^{-1}$  at 850 mb (left) and 200 mb (right) for CSM1 (top) and the difference between CSM1 and CCM3 (bottom).

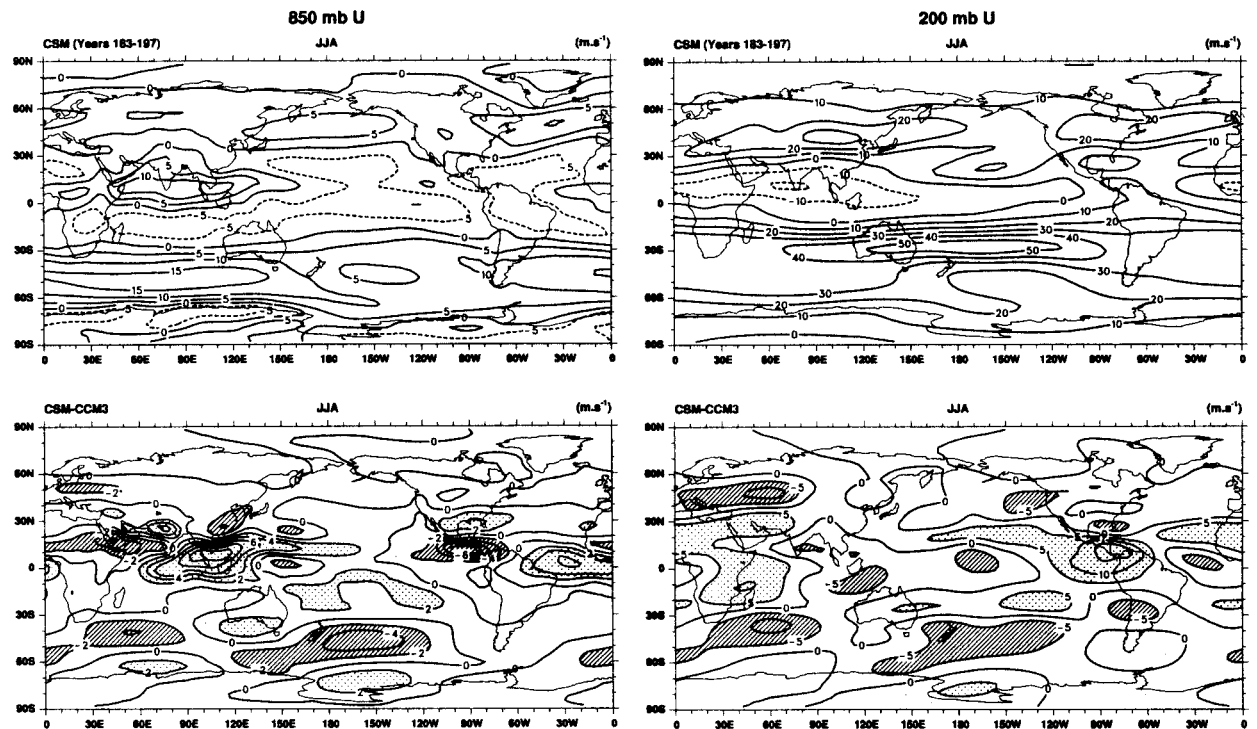


FIG. 12. As in Fig. 11 except for JJA.



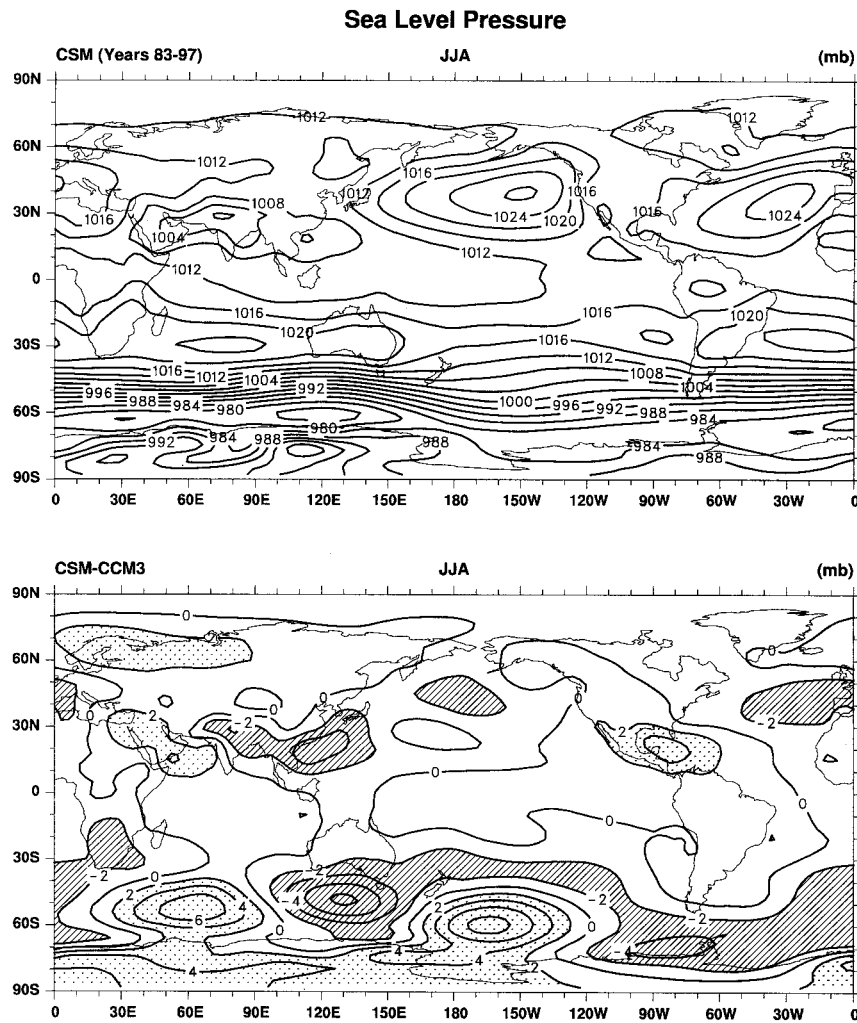


FIG. 14. As in Fig. 13 except for JJA.

precipitation shifts in both the tropical Pacific and Indian Oceans.

The differences in sea level pressure are considerably larger in the SH during JJA. Consistent with the differences in zonal winds (Fig. 12) there is a pronounced wave 2 pattern to the difference in the middle latitudes of the SH, where the influence of the ice distribution is strong. The differences in the SH quasi-stationary waves between CSM1 and CCM3 are discussed more extensively in Raphael (1998). The pressure is higher over the Caribbean and the Arabian Peninsula, where the precipitation is strongly reduced in CSM1, and lower over the Philippines, where the precipitation is stronger.

The differences in sea surface stresses (Figs. 15 and 16) are again largest in higher latitudes in winter, associated with the changes in sea level pressure and in the sea-ice distribution. In DJF the stress magnitudes are larger in both the North Pacific and the North Atlantic–Greenland Sea with the largest increases corresponding to the regions of increased ice cover in CSM1.

This difference is exaggerated because the surface stresses are too large over sea ice (see Weatherly et al. 1998). The surface stress equation over sea ice is the same in both models, but the increased ice in CSM1 gives a larger region of elevated stress. The zonally averaged zonal stress is larger in CSM1 between 50° and 60°N. In JJA, the surface stresses are weaker in CSM1 over the the middle- and high-latitude southern oceans, both because of the decrease in ice area and because of the change in low-level winds and sea level pressure. The wave 2 pattern found in the pressure differences is readily apparent in the surface stress differences as well. Significant differences are also found in the tropical Pacific and Indian Oceans (see Kiehl 1998), with CSM1 stresses generally larger than CCM3 stresses.

#### 4. Summary

The atmospheric simulation produced by CSM1, in which SSTs are generated by an ocean GCM coupled

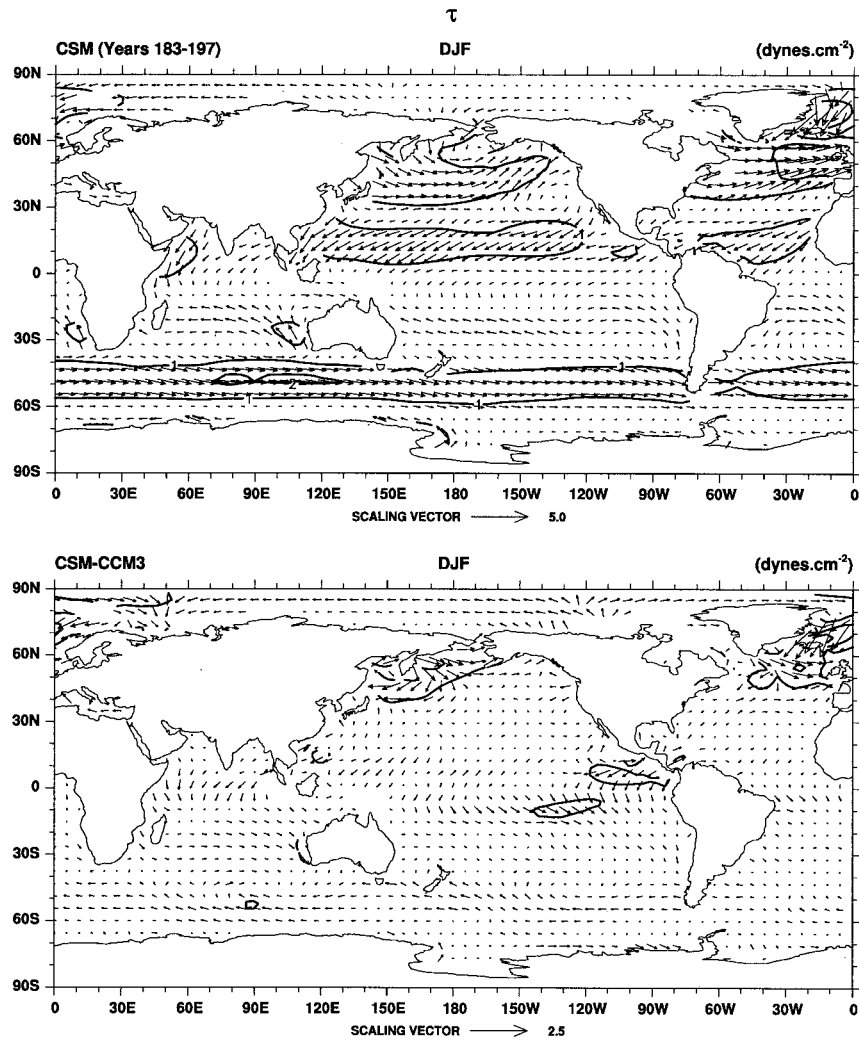


FIG. 15. Maps of DJF surface stress vectors over oceans and sea ice, for CSM1 (top), magnitudes contoured at 1 Pa, and the difference between CCM3 and CSM1 (bottom), magnitudes contoured at 0.5 Pa.

to CCM3, has been compared to a CCM3 simulation in which the SSTs were specified from observations. Differences between the simulations are remarkably small. The scarcity of large differences between the two simulated atmospheres is a consequence of the accuracy of the SST and sea-ice simulations in CSM1. The largest differences in temperatures occur over high latitudes in winter, associated with differences in sea ice. In the NH, the CSM1 simulated sea ice is too thick and too extensive, resulting in surface and lower-tropospheric temperatures that are too cold. In the Southern Hemisphere, the CCM3 diagnosed sea ice is too thick and too extensive, with similar effects on temperature. Partly because sea-ice extent strongly affects the surface albedo, the NH is, on average, slightly colder in CSM1 than in CCM3, while the SH is slightly warmer.

Tropical precipitation is significantly different in CSM1 compared to CCM3, particularly in southern

summer when considerably more precipitation occurs south of the equator in CSM1. In fact, neither CSM1 nor CCM3 appears to produce an extremely accurate simulation of the tropical precipitation in DJF and they lie on opposite sides of the observations.

The time-averaged net heat flux at the ocean surface in the coupled model must be balanced by heat transports within the ocean to maintain the time-averaged SST. In contrast, the ocean is assumed to have infinite heat capacity in the uncoupled model with specified SSTs. The uncoupled model can sustain large net heat fluxes into the atmosphere, largely in the form of latent heat, where such fluxes could not be supported by realistic ocean heat transport. Conversely, the calculated net heat flux in the uncoupled model may be small compared to the heat flux convergence in the real ocean. Thus, even modest errors in the physical parameterizations (or in dynamics) can give rise to large errors in

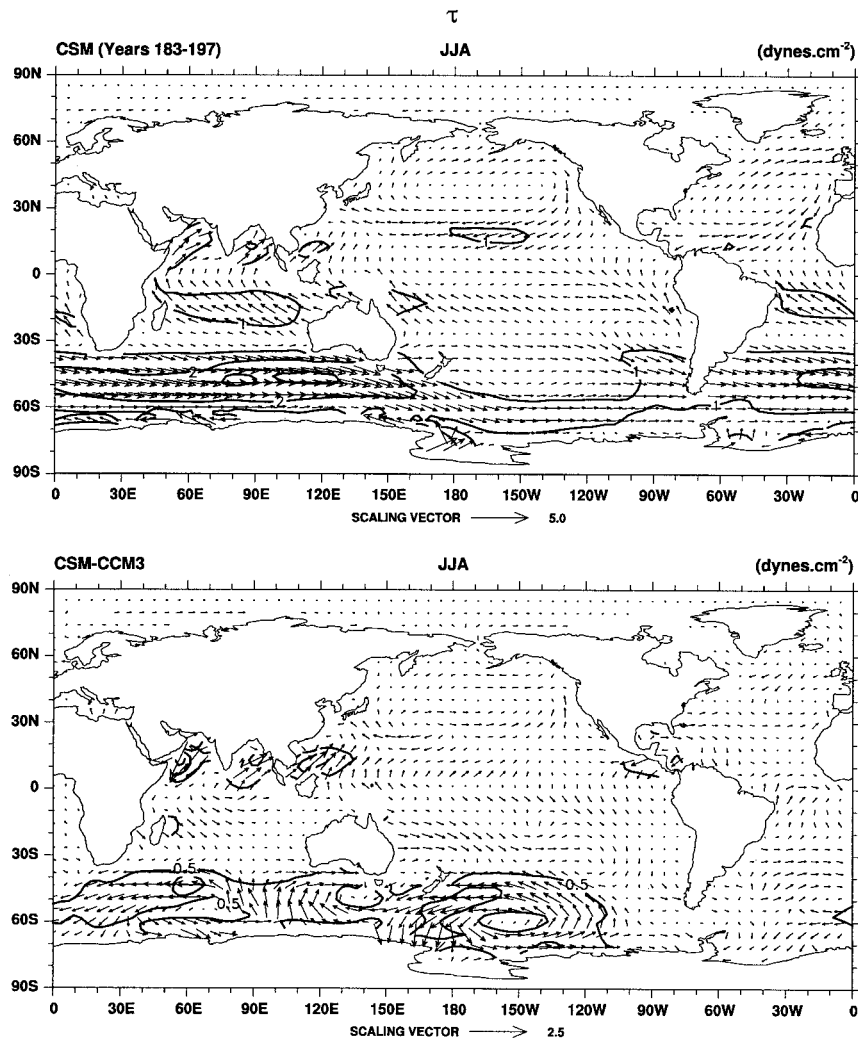


FIG. 16. As in Fig. 15 except for JJA.

latent heat flux and, eventually, in precipitation. When the atmosphere is coupled to the ocean, the SST must adjust until the net fluxes are balanced by ocean heat transport. Thus surface flux errors in the uncoupled model are largely converted into SST errors in the coupled model. However, this process is highly nonlocal, particularly in the Tropics, since it alters the SST gradients and precipitation distributions, resulting in feedbacks on the large-scale circulation.

The precipitation in both CSM1 and CCM3 appears to be too large (note that the simulated curves in Fig. 4 lie almost entirely above the satellite estimates), suggesting that the hydrologic budget is too vigorous, although weaker than in previous versions of the CCM. The globally and annually averaged precipitation is  $3.04 \text{ mm day}^{-1}$  in CSM1 and  $3.09 \text{ mm day}^{-1}$  in CCM3, corresponding to latent heat fluxes of  $88 \text{ W m}^{-2}$ , respectively. Observational estimates vary widely, but recent estimates of the latent heat flux are  $78 \text{ W m}^{-2}$  (Kiehl and Trenberth 1997), corresponding to a precip-

itation rate of  $2.7 \text{ mm day}^{-1}$ . The only way to decrease the precipitation is to decrease the latent heat flux from the oceans into the atmosphere. Since the oceans must balance their heat budget, this requires either decreasing the solar radiation absorbed in the oceans or increasing the downward longwave radiation (or both). The top of atmosphere radiative budget agrees fairly well with Earth Radiation Budget Experiment analyses (Kiehl et al. 1998), suggesting that decreasing the insolation absorbed in the oceans would require absorbing more in the atmosphere, rather than increasing cloudiness to reflect more back to space.

Significant differences in the winds are confined largely to the Tropics in response to the precipitation and latent heat release changes. Modest differences are found in middle and high latitudes in winter and appear to be associated more with sea ice changes in CSM1 than with tropical precipitation changes. The sea ice simulated in CSM1 is actually in better agreement with observations than is the diagnosed ice in CCM3, and

the higher-latitude SH circulation changes generally represent an improvement in CSM1. The opposite is true in the NH.

*Acknowledgments.* Many scientists in the Climate and Global Dynamics Division at NCAR contributed to the development of CSM1 and CCM3. The authors are grateful to them and especially to Thomas Bettge, Lawrence Buja, Brian Kauffman, Nancy Norton, James Ronsinski, John Truesdale, and Mariana Vertenstein, the software engineers primarily responsible for the development of the models. The NCAR Climate System Model would not have been built without the leadership and financial support from Jay Fein at the National Science Foundation.

## REFERENCES

- Bonan, G., 1998: The land surface climatology of the NCAR Land Surface Model (LSM 1.0) coupled to the NCAR Community Climate Model (CCM3). *J. Climate*, **11**, 1307–1326.
- Boville, B. A., and P. R. Gent, 1998: The NCAR Climate System Model, version one. *J. Climate*, **11**, 1115–1130.
- Briegleb, B. P., and D. H. Bromwich, 1998a: Polar radiation budgets of the NCAR CCM3. *J. Climate*, **11**, 1246–1269.
- , and —, 1998b: Polar climate simulation of the NCAR CCM3. *J. Climate*, **11**, 1270–1286.
- Bryan, F. O., 1998: Climate drift in a multicentury integration of the NCAR Climate System Model. *J. Climate*, **11**, 1457–1473.
- Flato, G. M., and W. D. Hibler, 1992: Modeling ice pack as a cavitating fluid. *J. Phys. Oceanogr.*, **22**, 626–651.
- Gates, W. L., 1992: AMIP: The Atmospheric Model Intercomparison Project. *Bull. Amer. Meteor. Soc.*, **72**, 1962–1970.
- Gent, P. R., J. Willebrand, T. J. McDougall, and J. C. McWilliams, 1995: Parameterizing eddy-induced tracer transports in ocean circulation models. *J. Phys. Oceanogr.*, **25**, 463–474.
- , F. O. Bryan, G. Danabasoglu, S. C. Doney, W. R. Holland, W. G. Large, and J. C. McWilliams, 1998: The NCAR Climate System Model global ocean component. *J. Climate*, **11**, 1287–1306.
- Hack, J. J., 1994: Parameterization of moist convection in the NCAR Community Climate Model (CCM2). *J. Geophys. Res.*, **99**, 5551–5568.
- , J. T. Kiehl, and J. W. Hurrell, 1998: The hydrologic and thermodynamic structure of the NCAR CCM3. *J. Climate*, **11**, 1179–1206.
- Holtslag, A. A. M., and B. A. Boville, 1993: Local versus non-local boundary layer diffusion in a global climate model. *J. Climate*, **6**, 1825–1842.
- Hurrell, J. W., J. J. Hack, B. A. Boville, D. Williamson, and J. T. Kiehl, 1998: The dynamical simulation of the NCAR Community Climate Model version 3 (CCM3). *J. Climate*, **11**, 1207–1236.
- Kiehl, J. T., 1998: Simulation of the tropical Pacific warm pool with the NCAR CSM. *J. Climate*, **11**, 1342–1355.
- , and K. E. Trenberth, 1997: Earth's annual global energy budget. *Bull. Amer. Meteor. Soc.*, **78**, 197–208.
- , J. J. Hack, G. Bonan, B. A. Boville, D. Williamson, and P. Rasch, 1998a: The National Center for Atmospheric Research Community Climate Model: CCM3. *J. Climate*, **11**, 1131–1149.
- , —, and J. W. Hurrell, 1998b: The energy budget of the NCAR Community Climate Model: CCM3. *J. Climate*, **11**, 1151–1178.
- Large, W. G., J. C. McWilliams, and S. C. Doney, 1994: Oceanic vertical mixing: A review and a model with a nonlocal boundary layer parameterization. *Rev. Geophys.*, **32**, 363–403.
- Mechoso, C. R., and Coauthors, 1995: The seasonal cycle over the tropical Pacific in coupled ocean–atmosphere general circulation models. *Mon. Wea. Rev.*, **123**, 2825–2838.
- Meehl, G. A., and J. Arblaster, 1998: The Asian–Australian monsoon and El Niño–Southern Oscillation in the NCAR Climate System Model. *J. Climate*, **11**, 1356–1385.
- Raphael, M., 1998: Quasi-stationary waves in the Southern Hemisphere: An examination of their simulation by the NCAR Climate System Model, with and without an interactive ocean. *J. Climate*, **11**, 1405–1418.
- Semtner, A. J., 1976: A model for the thermodynamic growth of sea ice in numerical investigations of climate. *J. Phys. Oceanogr.*, **6**, 379–389.
- Weatherly, J., B. Briegleb, W. G. Large, and T. Bettge, 1998: Sea ice and polar climate in the NCAR CSM. *J. Climate*, **11**, 1472–1486.
- Xie, P., and P. A. Arkin, 1996: Analyses of global monthly precipitation using gauge observations, satellite estimates and numerical model predictions. *J. Climate*, **9**, 840–858.
- Zhang, G. J., and N. A. McFarlane, 1995: Sensitivity of climate simulations to the parameterization of cumulus convection in the Canadian Climate Centre general circulation model. *Atmos.–Ocean*, **33**, 407–446.